FEM heat transfer modelling with tomography-based SiC_f/SiC unit cell

Andrea Cavaliere[1], Federica Marone[2], Cedric Cozzo[3], Karl Buchanan[4], Christophe Lorrette[5], Manuel A. Pouchon[1]*

[1]Laboratory for Nuclear Materials, Paul Scherrer Institut, Forschungstrasse 111, Villigen, Switzerland
[2] Swiss Light Source, Paul Scherrer Institut, Forschungstrasse 111, Villigen, Switzerland
[3]Laboratory for Reactor Physics and Thermal-hydraulics, Paul Scherrer Institut, Forschungstrasse 111, Villigen, Switzerland
[4]Framatome, Fuel Design, 2 rue Professeur Jean Bernard, 69007, Lyon, France
[5]Université Paris-Saclay, CEA, Service de Recherches Métallurgiques Appliquées, 91191, Gif-sur-Yvette, France

Abstract

Modern industry has become increasingly reliant on composite materials for a variety of applications, and the nuclear industry is no exception to this. Among the materials being researched as Enhanced Accident Tolerant Fuels, ceramic matrix composites such as SiC-fiber-reinforced SiC (SiC_f/SiC) figure as some prime candidates due to their excellent high temperature performances. SiC_f/SiC so far shows adequate nuclear, mechanical and chemical properties; still, the thermal properties need further investigation.
The thermal behavior of a material is an important factor for its performance as a nuclear fuel cladding, i.e. the first barrier encapsulating the fuel pellets. Many features determine the resulting properties of composite materials, such as matrix and fiber reinforcement properties and orientation, void fraction, and pore morphology. This study establishes a methodology to study the physical properties of composite materials and applies it to SiC_f/SiC. A FEM model is used to characterize the thermal properties of a fundamental SiC_f/SiC element, referred to as a "unit cell", with the objective of accurately predicting the thermal properties of this complex class of materials where experimental data is often difficult to obtain. The unit cell is built based on data acquired with high-resolution tomographic microscopy performed at the TOMCAT beamline of the Swiss Light Source.
By using phase-retrieval prior to tomographic reconstruction, the pores, fibers and matrix that compose the material can be distinguished in the data analysis. The separated information is processed to obtain geometrical information about the individual pores and fibers, which is then used to parametrize them as cylindrical objects. This allows constructing a FEM model of a cubic unit cell that is used to extract the effective thermal properties of SiC_f/SiC. The analysis scheme includes steady-state and dynamic thermal transport simulations, which yield directional effective thermal conductivity and diffusivity values, respectively. Both modes of analysis show isotropic thermal conductivity values in the range of 71 W/m/K at room temperature, more than three times that of currently employed nuclear cladding materials.
Combining these results with the data on the larger structural features of the material will lead to realistic results on the macroscopic thermal properties.

* Corresponding author: andrea.cavaliere@psi.ch

Keywords:
Accident Tolerant Fuels
Finite Element Method
Ceramic matrix composite
Silicon Carbide
Nuclear fuel cladding
Synchrotron tomography
Thermal conductivity
Laser flash

1 INTRODUCTION

The reality of climate change creates an ever-growing need for a restructuring of the energy industry, with low-carbon sources at its core. Despite having an excellent safety and operational record [1], nuclear energy is not endorsed everywhere as public opinion has been deeply influenced by the nuclear accident that took place in Fukushima, Japan, in March 2011, triggered by a catastrophic combination of an earthquake and tsunami.
After extended exposure to high temperature, the cladding material (a Zr alloy by the name of "Zircaloy") underwent the well-known breakaway oxidation that leads to an increase of hydrogen production, which caused the explosion in the reactor building.
In order to prevent or reduce the production of combustible gas in accidental conditions, a branch of the research on nuclear materials focuses on alternative materials for fuel and cladding, called "Accident Tolerant Fuels" (ATFs) [2]. This line of research has received renewed support after the Fukushima accident. This line of research has received renewed support after the Fukushima accident. There are several ATF concepts for both new fuels and fuel claddings [1], [3]. They can be categorized as "evolutionary", when they try to improve on currently employed materials (e.g. Cr-coated Zr cladding), or "revolutionary", when they propose to replace mature solution with a breakthrough materials (e.g. SiC_f/SiC, a ceramic matrix composite (CMC) consisting of a SiC matrix reinforced by SiC fibers).
This study is part of a research project for the thermophysical characterization of SiC_f/SiC, a revolutionary ATF cladding concept with a particularly complex internal structure compared to metallic claddings. In the broader context of composite material research, this study also aims to establish a methodology for the physical characterization of composite materials based on a combination of tomography and Finite Element Method (FEM) modelling. While SiC has a history of use in the nuclear industry [4] and adequate nuclear and mechanical properties, its thermal properties are still under investigation. In particular, thermal conductivity of the cladding material is a key property in determining the efficiency with which heat can be transferred from the nuclear fuel pellets to the cooling water. The thermal conductivity of monolithic SiC is very high, up to 400 W/m/K depending on the microstructure and purity [5], however in the case of the composite SiC the introduction of fibers generates a complex network of intra/inter yarns porosity and various interfaces which significantly affect the thermal properties.
Detailed information on the internal structure could greatly improve our understanding of SiC_f/SiC composites. In this study, synchrotron tomographic microscopy at the TOMCAT beamline of the Swiss Light Source (SLS) is employed to reconstruct the internal features of this material in high resolution. The results are processed to create a microscopic sample of the material, referred to as the "unit cell", which is characterized with a FEM model. Two modes of analysis are proposed: the steady state analysis, where the unit cell's equilibrium under fixed thermal loads is studied, and transient analysis, which is modelled after a laser flash experiment, where the propagation of a thermal pulse in the unit cell is measured. Both methods are aimed at reconstructing the effective thermal conductivity of the material.

The characterization of the unit cell is one step in an extensive study of the material. This includes macroscopic simulations to evaluate the response at characteristic lengths of the cladding thickness, and the development of an experimental setup for the thermophysical characterization of tubular samples, which will be used to validate the results of the simulations.

2 MATERIALS AND METHODS

2.1 Sample characteristics

The material under investigation is CMC SiC, reinforced by Hi-Nicalon Type S (HNS) SiC fibers, deemed to be of nuclear-grade fibers which present high thermal stability, high creep and oxidation resistance [6]. The mean diameter of the fibers is 13 μm, they are covered with a Pyrolytic Carbon (PyC) coating of about 30 nm to mechanically separate them from the matrix. In the first step of the production, the fibers are shaped into a cylindrical preform with two non-interlocked layers: a first layer of helical wound fibers at a ± 45° angle with the tube's axis and a second layer of 2D braided fibers again with a ± 45° angle with the tube's axis. Afterwards, the SiC matrix is densified by Chemical Vapor Infiltration (CVI) before applying internal and external smoothing surface treatments. More details on the manufacturing process are given by *Braun et al.* [7]. The final product is a dense solid tube with reinforcement having a certain level of porosity, evaluated at 6.1% for the sample characterized in this study. This material design is jointly developed and produced by CEA with the support of Framatome. Advances in recent years have enabled the production of a new generation of CVI-SiC_f/SiC composites exhibiting a lower porosity. A picture of the analyzed sample is shown in Figure 1.

Figure 1: SiC_f/SiC sample analyzed in this study.

2.2 Synchrotron tomographic microscopy

Synchrotron tomographic microscopy at the TOMCAT beamline of the Swiss Light Source was used to investigate the internal structure, with the additional use of propagation-based phase contrast [8]. With this technique, it is possible to increase contrast exploiting not only X-ray absorption differences, but also the phase shift induced on the beam by interfaces in the sample, allowing to reconstruct even small density variations in the materials. The feasibility of discriminating between fiber and matrix in this material has already been reported in literature [9]. Leveraging on phase contrast is crucial to clearly differentiate the matrix, the fibers and the pores in the material, as seen in Figure 2. In this study, we consider the results of the scans taken at a 10x magnification at the beamline, which corresponds to a pixel size of 0.65 μm/px. These scans were performed with a photon energy of 25 keV and a measurement time per projection of 300 ms. For each scan, 1001 projections were acquired. This resolution allows to fully reconstruct the fibers and the majority of the pores, but it may not resolve sub-micron features at the matrix-fiber interface.

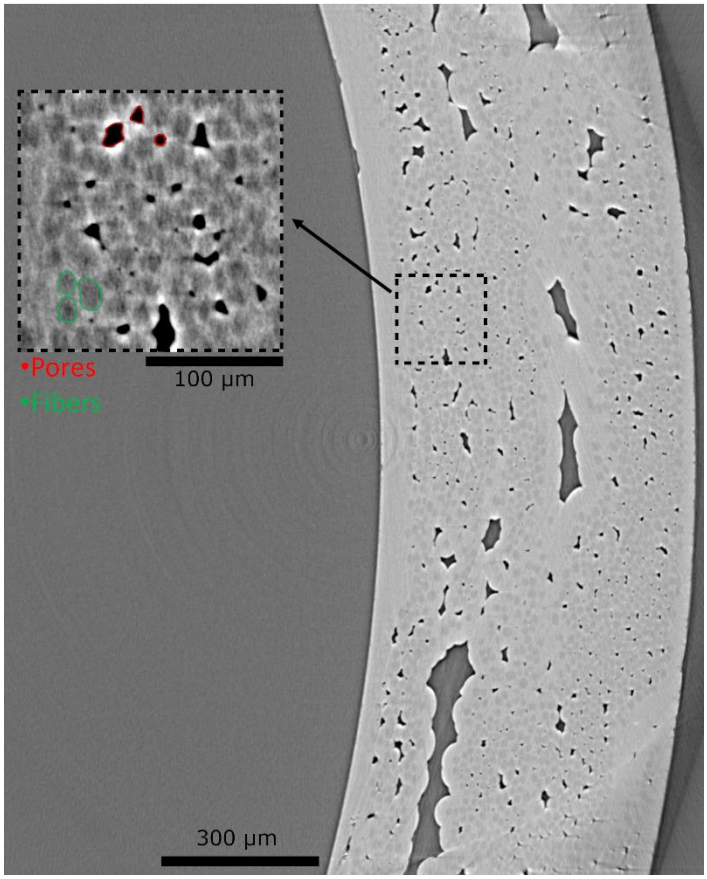

Figure 2: Tomography reconstruction image of the SiC_f/SiC sample. A contrast-enhanced close up shows the fibers and the pores clearly.

The open-source software Fiji was used to process the images [10]. A selected square region, with a side of ca. 100 µm, was cut out for 150 images in the stack, and the contrast adjusted to maximize the visibility of the fibers. The segmentation was performed with the Trainable Weka Segmentation tool in the Fiji toolset [11]. This plugin is based on the Weka machine learning package, and it allows to apply machine learning to the task. By manually populating three classes with the regions in the image corresponding to pores, fibers and matrix, a classifier is trained to automatically separate the three materials in the image. Multiple training parameters can be specified, concerning edge detection, noise reduction and membrane reconstruction. The training has been repeated multiple times, by correcting the errors in the segmentation, until no noticeable improvement in the result was visible. The segmentation produces an image in three colors, one for each class entered by the user, which can then be further decomposed with Fiji into three separate binary images, containing the individual data for each class (Figure 3).

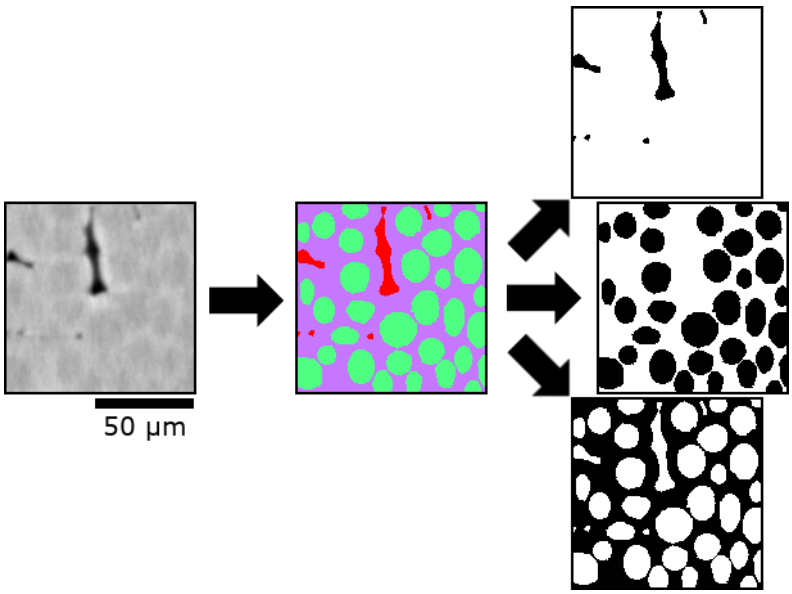

Figure 3: Example of the application of the WEKA segmentation. The input image is processed by the machine learning algorithms, which classify the pixels as belonging to pores (red), fibers (green) or the matrix (magenta). The resulting tricolored image can then be split into three binary images with information solely on one specific phase.

2.3Reconstructing 3D objects

The objective of the image processing is to prepare data sets that can be used to create a unit cell of SiC_f/SiC, which can be processed in FEM simulations. In our approach, pores and fibers are replaced with parametrized 3D shapes. Both pores and fibers in the material, specifically inside a fiber bundle, are very elongated and exhibit little variation in the diameter, as shown in Figure 4. For these reasons, cylinders are deemed adequate representations of pores and fibers.

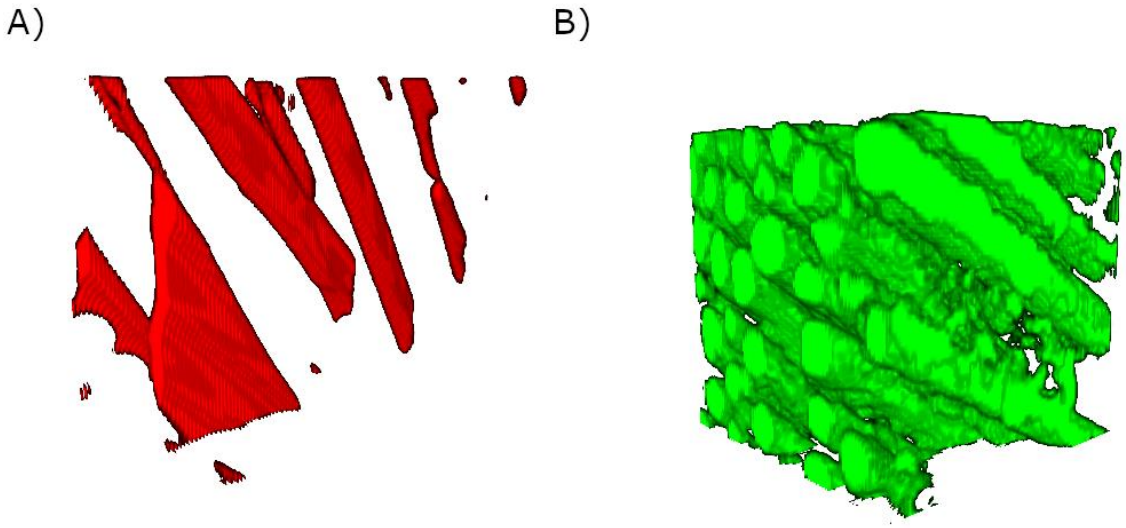

Figure 4: Three dimensional renderings of the internal features of the material: A) pores; B) fibers.

Two Python scripts were developed to reconstruct the pores and fibers as individual objects and to measure their geometrical characteristics. This provides dimensions, position and orientation values with which equivalent cylinders can be created.
The first script analyzes a stack of images, to group together voxels belonging to the same object, be it a pore or a fiber. To start, it analyzes the first image in the stack, and groups

together adjacent voxels, creating the first set of individual objects. Then, it continues to the next image, where the process is repeated. The script then checks for the presence of overlapping objects in the two images. If there are any, they are condensed into a single entity. The two object lists are cross-checked multiple times, to ensure that bifurcating pores are reconstructed correctly. Once this step is finished, the script continues loading and processing the next images in the stack until there are no more, and the pores and fibers are reconstructed fully as 3D entities, represented by a collection of Cartesian coordinates for voxels they are made of.
The second script analyses the 3D objects with singular value decomposition, returning the main orientation. The determined direction is then used to measure the length, width, and orientation angle of the object, as well as end points that would serve as extremities of the central axis of a cylinder.

2.4FEM model

The system is modelled and meshed with GMSH, an open-source 3D mesh generator [12]. The results of the analysis code can be used to build an input file, which instructs the software on how to build a cube for the SiC matrix body and cylinders for pores and fibers. The volumes for the latter features are then subtracted with a Boolean operation from the cube, to avoid overlapping volumes of different bodies. The resulting mesh is shown in Figure 5. It should be noted that the smaller, spherical pores, of less than 100 voxels in size (ca. 3 µm in diameter if approximated as spheres), are not modelled directly as cylinders. Instead, they are homogenized in the matrix material, and treated as a reduction in the density and thermal conductivity of the matrix based on Loeb's relation [13]:

$$k = k_m(1 - \nu_p), \tag{1}$$

where k_m is the thermal conductivity of the matrix material and ν_p is the pore volume fraction.

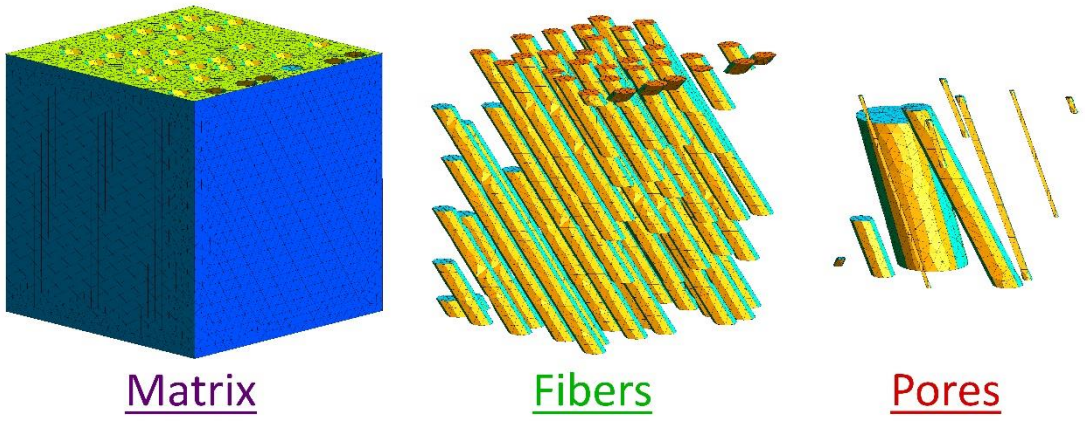

Figure 5: Mesh structure of the FEM simulation. Three main materials make up the system: SiC matrix (modelled as a cube with some volumes removed), SiC fibers (modelled as cylinders) and pores (modelled as cylinders).

Table 1: Physical parameters of the matrix, fibers and pores (assumed air filled) that are used in the FEM model of the SiC$_f$/SiC unit cell (data extracted from Ref [5], [14]).

	k [W/m/K]	ρ [kg/m^3]	c_p [J/kg/K] @ 300 K

Matrix	90	3215	692
Fibers	18.4	3100	692
Pores	0.024	1.225	1004

For the FEM simulation, the open-source multiphysical solver Elmer is used [15]. The three materials that make up the unit cell are defined in the software with the parameters shown in Table 1. The densities and thermal conductivities of the SiC matrix and fibers were taken from [5] and [14] respectively. It should be noted that the specific heat of the matrix and fibers is based on an interpolation of the experimental values found in the 1970 data book [16]. The best fitting interpolation is found to be the root fit polynomial shown in equation (2):

$$c_p(T) = 0.2 \cdot T - 179.0 \cdot T^{\frac{1}{2}} + 896.9 \cdot T^{\frac{1}{3}} - 2271.5, \tag{2}$$

where c_p is the specific heat expressed in W/m/K and the temperature is expressed in K. This fit shows very good agreement with the reference data, with an R-squared value of 99.4% and no evidence of overfitting within the reference data range.

Individual bodies are defined for each fiber and pore, while a single body is created for the matrix. The solver is called to solve equation "HeatSolverVec" in Elmer. This new solver for the heat equation is designed to include the master-slave system with the Discontinuous Galerkin method to treat heat transfer at an interface [17]. This method allows to impose a virtual heat transfer coefficient α at an interface, which is used to model a resistance to heat flow. The heat transfer coefficient is enforced as a boundary condition between the matrix and the fiber material, and it is set equal to 10 W/m/K. This is consistent with the available data on the thermal conductivity of a PyC coating [18], [19], and it reflects the impeding nature of the interface. Indeed the PyC structure consists of parallel layers of graphene planes, whose thermal conductivity is very high in-plane (hundreds of W/m/K) but much lower out-of-plane (ca. 10 W/m/K). Given that the PyC interphase is deposited parallel to the fibers, the conductivity through the interface would conform to the lower values.

It should be noted that with the small scale of the simulations, phonon ballistic phenomena may play an important role, given the phonon mean free path of ca. 523 nm in 3C-SiC [20]. The accuracy of these simulations could thus be improved by implementing a model for these phenomena, as *Lee et al.* do with the use of the Extended Finite Element Method [21]. Introducing models for poor matrix-fiber contact, as in *Klett et al.* [22], could complement the model nicely, by including more features that can cause phonon scattering and by allowing to account for any unresolved structure at the fiber-matrix interface.

The pores are assumed to be air-filled at atmospheric pressure. For this reason, it is important to determine the active modes of heat transfer through them. By calculating the Rayleigh number *Ra*, it is possible to determine whether the condition for stability of convection is met. For parallel infinite planes, this occurs for $Ra > 1708$ [23]. This number can be calculated with equation (3):

$$Ra_x = \frac{g \cdot \beta}{\nu \cdot \alpha}\left(T_s - T_{inf}\right) \cdot x^3, \tag{3}$$

where the parameters represent:

- g : gravity of Earth = 9.81 m/s^2
- β : thermal expansion coefficient (K^{-1})
- ν : kinematic viscosity (m^2/s)
- α : thermal diffusivity (m^2/s)
- T_s : surface temperature (K)
- T_{inf} : quiescent temperature (K)

- x : characteristic length (m)

Table 2: Rayleigh number for various characteristic lengths.

x [µm]	1	10	100	1000	6731
Ra_x	5.6e-9	5.6e-6	5.6e-3	5.6	1708

For a temperature difference of 50 K, which is more than expected for these small pores, the Rayleigh number is calculated and tabulated for various characteristics lengths in Table 2. It is shown that the critical value is reached for x = 6731.3 µm. Given that the maximum width and length of the analyzed pores are respectively 39 µm and 298 µm, convection can be considered negligible. Thus, heat transfer is modelled solely with conduction and radiative heat transfer, the latter using diffuse grey radiation.

2.5Modes of analysis

Based on the usual practices described in [24]–[26], two modes of analysis of the unit cell are proposed. The first mode is a steady state analysis of the thermal equilibrium. A heat flux boundary condition of 10^8 W/m^2 is set on one side of the cubic unit cell (leading to approximately 1 W of total power on that surface), while on the opposite side the temperature is fixed at 273 K. All other surfaces are made adiabatic. By measuring the average temperature at equilibrium on the two surfaces and rearranging Fourier's law of heat conduction, it is easily possible to calculate the thermal conductivity with equation (4):

$$k_x = q_x \frac{\Delta x}{\Delta T}, \tag{4}$$

where k_x is the thermal conductivity along the x-axis, q_x is the heat flux term, Δx is the distance between the two surfaces and ΔT is the temperature difference.

The second mode of analysis is a simulated laser flash experiment. Laser flash is a well-established technique to measure the thermal diffusivity of a material. A thermal pulse is initiated on one side of the unit cell, and on the opposite side the evolution of temperature in time (i.e. the thermogram) is recorded. Based on the theory developed by *Parker et al.* [27], it is possible to derive the thermal diffusivity α of a material with the half-rise time $t_{\frac{1}{2}}$ of the thermogram, by using equation (5):

$$\alpha = \left(\frac{1.38 L^2}{\pi^2 t_{\frac{1}{2}}} \right), \tag{5}$$

where L is the distance between the heated surface and the rear-surface (where the thermogram is recorded). The knowledge of the density ρ and the specific heat c_p of the material allow the determination of the effective thermal conductivity with equation (6):

$$k = \alpha \rho c_p, \tag{6}$$

3 RESULTS AND DISCUSSION

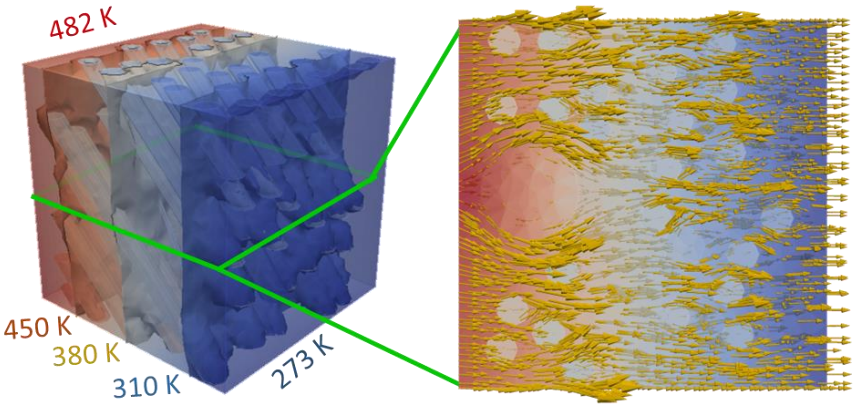

Figure 6: Volumetric rendering of the results obtained with a steady state simulation of the thermal behavior of the unit cell, with several highlighted temperature isosurfaces. The cutout section shows the thermal barrier behavior of the pores and fibers.

Table 3: Results of the steady-state (SS) and laser flash (LF) simulations of the thermal behavior of the SiC$_f$/SiC unit cell. The thermal conductivity is evaluated along the three main axes of the cell.

	X	**Y**	**Z**
SS: k_{eff} [W/m/K]	70.8	71.6	71.1
LF: k_{eff} [W/m/K]	72.3	72.3	73.1

The results of the simulations are tabulated in Table 3 and rendered in Figure 6 with ParaView [28]. The two modes of analysis employed provided consistent results, and both show that the behavior along the considered directions is isotropic. The small differences between the two sets of simulations might be caused by the difference in maximum temperature obtained within them (482 K for the SS mode, 460 K for the LF), which leads to slightly different values for the specific heat. Also, a sensitivity study was conducted to determine the influence of the heat transfer coefficient α on the effective thermal conductivity of the unit cell. The results show that it ranged between 69.6 W/m/K and 74.1 W/m/K, showing how little this parameter affects the overall properties of the material in this specific simulation. Thus, for the microscopic unit cell, the results show thermal conductivities more than three times higher than those of Zr-based claddings and other ATF concepts such as FeCrAl [29], [30] providing additional margin to accommodate the expected decrease under irradiation.

Overall, the thermal barrier effect from pores and fibers is identified in the volumetric rendering, with a reduction of the conductivity of the matrix material between 20.4 % and 21.3 %. It is possible to compare these results with the upper bound of the rule of mixtures, which assumes the material's components to act as parallel thermal resistances, with equation (7):

$$k_{eff} = k_m v_m + k_f v_f + k_p v_p = 57.1 \frac{W}{m \cdot K}, \tag{7}$$

where k_i and v_i represent the thermal conductivity and the volume fraction of each phase, respectively. These values are calculated for this specific unit cell and listed in Table 4. The share variation of each component in a slice stack of the material is also reported in Figure 7. The rule of mixtures underestimates the thermal conductivity of this material however, due to the fact that it does not account for the radiative heat transfer that occurs through

pores and due to the high volume fraction of fibers, which may invalidate the assumption of non-interacting dispersed phases.

Table 4: Volume fractions and thermal conductivities of the material's components in the unit cell [5], [14].

	Pores	**Fibers**	**Matrix**
ν [%]	3.8	41.1	55.1
k [W/m/K]	0.024	18.4	90

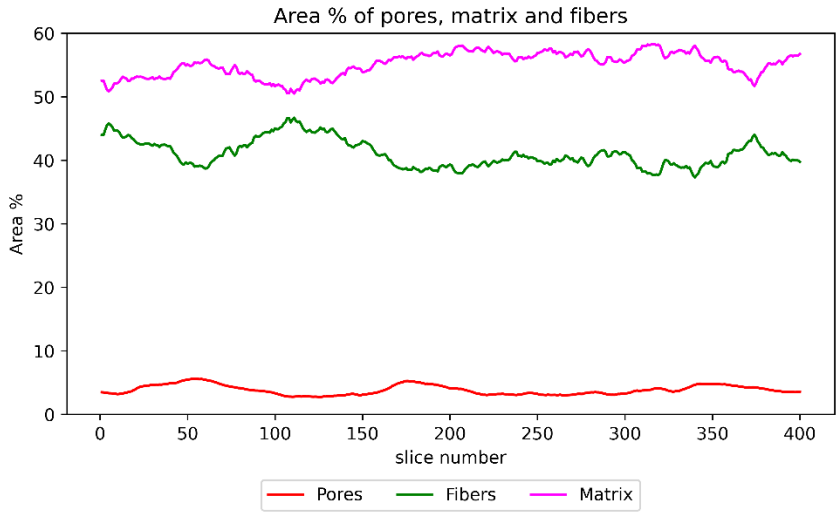

Figure 7: Area percentage of pores matrix and fibers for 400 slices of material, with the same size and in the same location as those used for the unit cell reconstruction.

The thermal conductivity of SiC_f/SiC is heavily dependent on fiber type and architecture, matrix material properties, and characteristics of the interphase. There are large variations in the reported room temperature thermal conductivity values, but they mostly lie in the 15 – 25 W/m/K range, with few above 35 W/m/K or below 10 W/m/K [1], [14], [18], [31]–[35]. Results pertaining to this specific material are described by *Duquesne et al.* [33]–[35], with values in the 28 – 32 W/m/K range. The level of porosity strongly affects these results, as shown by *Tao and Wang* [32]. Figure 8 shows the area-weighted pore size distribution in the 2D tomography slices of the sample. The variety in pores sizes is a consequence of the complex network related to the fibrous architecture, with pores forming both inside and in-between fiber bundles during the matrix densification process. With this cubic unit cell, with a 100 µm side, the larger pores cannot be taken into account, thus a lower thermal conductivity is expected when considering all features; this will be analyzed with a larger model of the material in a future study.

Lastly, due to the resolution limit, there is a lack of information on sub-micron porosity that might be present in the sample. In this model, the SiC matrix is assumed polycrystalline, with small grain, but if it contained unresolved porosity, the matrix thermal conductivity could be lower than assumed [5]. Still, thermoreflectance method has been used to probe the thermal conductivity of the various components of SiC_f/SiC, and the CVI matrix shows values around 100 W/m/K at room temperature [18], which justifies our assumption.

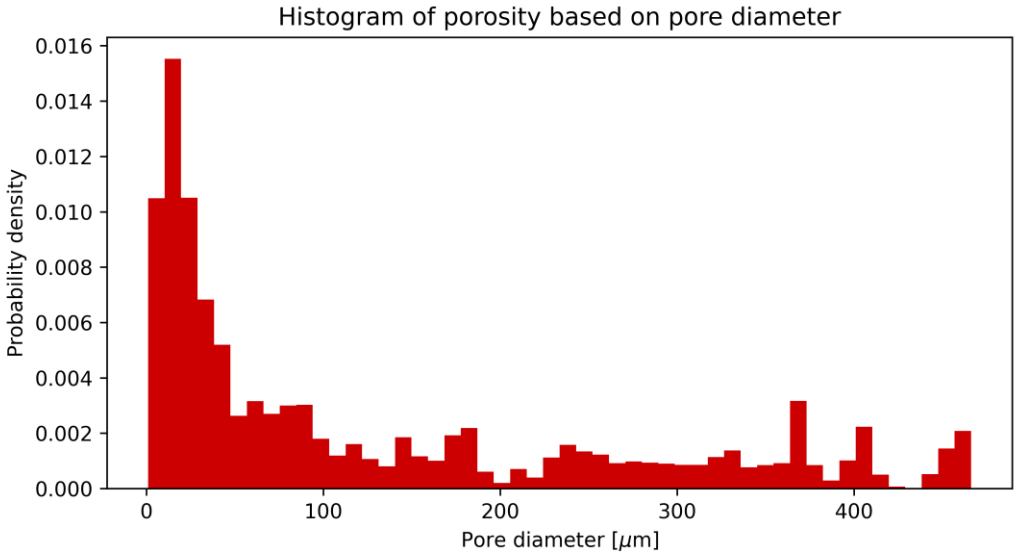

Figure 8: Area-weighted pore diameter histogram, showing the contribution of each class of pores to the total porosity.

4 CONCLUSION

Synchrotron tomographic microscopy has been performed in order to investigate the internal features of a SiC_f/SiC sample, with the purpose of using the data to build a unit cell of material for FEM simulation. Several features of interest have been highlighted and reconstructed as individual 3D objects with a Python reconstruction code. An analysis script has been used to measure the geometrical parameters of these 3D objects, which are then modelled as cylinders in the SiC_f/SiC unit cell. The unit cell has been characterized with two modes of analysis, steady state thermal analysis and simulated laser flash.

The developed methodology for the thermophysical characterization of the material with FEM simulations shows promising results. The final thermal conductivity values obtained in this study are higher than the usual experimental results for this material [31], but it should be noted that they are specifically focused on a microscopic unit cell, thus excluding the significant effect of the large pores. Furthermore, the imposition of a fixed thermal effective thermal conductivity at interface may not be sufficient to capture the complexity of phonon scattering at this scale. Improvements in the implementation of the interface effect with models for poor matrix-fiber contact and phonon ballistic phenomena may strongly improve the physical fidelity of the model. Still, if confirmed, these would be very promising values for a nuclear fuel cladding candidate. Finally, the work provided here offers an insight on the determination of an equivalent transverse conductivity, which is an important step in assessing the performance of SiC_f/SiC clad fuel rods.

This study will be used as a basis to build a macroscopic model of the behavior of the material, where the bulk properties will correspond with the values obtained with the unit cell characterization, and the large pores will be modelled directly. The results of the macroscopic simulation will be validated with a future experiment that is currently under development.

5 ACKNOWLEDGEMENTS

The project was funded in the frame of the IMAGO project. We acknowledge the Paul Scherrer Institut, Villigen, Switzerland for provision of synchrotron radiation beamtime at the TOMCAT beamline of the SLS.

6 BIBLIOGRAPHY

[1] Nuclear Energy Agency, *State-of-the-Art Report on Light Water Reactor Accident-Tolerant Fuels*. OECD, 2018. doi: 10.1787/9789264308343-en.

[2] K. A. Terrani, "Accident tolerant fuel cladding development: Promise, status, and challenges," *J. Nucl. Mater.*, vol. 501, pp. 13–30, Apr. 2018, doi: 10.1016/j.jnucmat.2017.12.043.

[3] "CSNI Technical Opinion Paper No. 19: Applicability of Nuclear Fuel Safety Criteria to Accident-tolerant Fuel Designs," p. 56.

[4] Y. Katoh and L. L. Snead, "Silicon carbide and its composites for nuclear applications – Historical overview," *J. Nucl. Mater.*, vol. 526, p. 151849, Dec. 2019, doi: 10.1016/j.jnucmat.2019.151849.

[5] L. L. Snead, T. Nozawa, Y. Katoh, T.-S. Byun, S. Kondo, and D. A. Petti, "Handbook of SiC properties for fuel performance modeling," *J. Nucl. Mater.*, vol. 371, no. 1–3, pp. 329–377, Sep. 2007, doi: 10.1016/j.jnucmat.2007.05.016.

[6] H. Ichikawa, "Recent advances in Nicalon ceramic fibres including Hi-Nicalon type S," *Ann. Chim. Sci. Matér.*, vol. 25, no. 7, pp. 523–528, Nov. 2000, doi: 10.1016/S0151-9107(01)80004-0.

[7] J. Braun, C. Sauder, J. Lamon, and F. Balbaud-Célérier, "Influence of an original manufacturing process on the properties and microstructure of SiC/SiC tubular composites," *Compos. Part Appl. Sci. Manuf.*, vol. 123, pp. 170–179, Aug. 2019, doi: 10.1016/j.compositesa.2019.04.031.

[8] D. Paganin, S. C. Mayo, T. E. Gureyev, P. R. Miller, and S. W. Wilkins, "Simultaneous phase and amplitude extraction from a single defocused image of a homogeneous object," *J. Microsc.*, vol. 206, no. 1, pp. 33–40, Apr. 2002, doi: 10.1046/j.1365-2818.2002.01010.x.

[9] Y. Gao *et al.*, "Synchrotron X-ray tomographic characterization of CVI engineered 2D-woven and 3D-braided SiCf/SiC composites," *Ceram. Int.*, vol. 42, no. 15, pp. 17137–17147, Nov. 2016, doi: 10.1016/j.ceramint.2016.08.001.

[10] C. A. Schneider, W. S. Rasband, and K. W. Eliceiri, "NIH Image to ImageJ: 25 years of image analysis," *Nat. Methods*, vol. 9, no. 7, pp. 671–675, Jul. 2012, doi: 10.1038/nmeth.2089.

[11] I. Arganda-Carreras *et al.*, "Trainable Weka Segmentation: a machine learning tool for microscopy pixel classification," *Bioinformatics*, vol. 33, no. 15, pp. 2424–2426, Aug. 2017, doi: 10.1093/bioinformatics/btx180.

[12] "[Gmsh] Mesh size definition referring to surface or volume numbers." http://onelab.info/pipermail/gmsh/2011/006436.html (accessed Apr. 16, 2020).

[13] D. S. Smith *et al.*, "Thermal conductivity of porous materials," *J. Mater. Res.*, vol. 28, no. 17, pp. 2260–2272, Sep. 2013, doi: 10.1557/jmr.2013.179.

[14] Y. Katoh *et al.*, "Continuous SiC fiber, CVI SiC matrix composites for nuclear applications: Properties and irradiation effects," *J. Nucl. Mater.*, vol. 448, no. 1–3, pp. 448–476, May 2014, doi: 10.1016/j.jnucmat.2013.06.040.

[15] J. Ruokolainen, M. Malinen, P. Råback, T. Zwinger, A. Pursula, and M. Byckling, *ElmerFEM - Open Source Multiphysical Simulation Software*. CSC - IT Center for Science (CSC). [Online]. Available: https://www.csc.fi/web/elmer/elmer

[16] Y. S. Touloukian and E. H. Buyco, "Thermophysical properties of matter - the TPRC data series. Volume 5. Specific heat - nonmetallic solids. (Reannouncement). Data book," Purdue Univ., Lafayette, IN (United States). Thermophysical and Electronic Properties Information Center, AD-A-951939/8/XAB, Jan. 1970. Accessed: Apr. 20,

2020. [Online]. Available: https://www.osti.gov/biblio/5303501-thermophysical-properties-matter-tprc-data-series-volume-specific-heat-nonmetallic-solids-reannouncement-data-book
[17] J. Ruokolainen, M. Malinen, P. Råback, T. Zwinger, A. Pursula, and M. Byckling, "ElmerSolver Manual," p. 163.
[18] E. K. Pek, J. Brethauer, and D. G. Cahill, "High spatial resolution thermal conductivity mapping of SiC/SiC composites," *J. Nucl. Mater.*, vol. 542, p. 152519, Dec. 2020, doi: 10.1016/j.jnucmat.2020.152519.
[19] E. López-Honorato, C. Chiritescu, P. Xiao, D. G. Cahill, G. Marsh, and T. J. Abram, "Thermal conductivity mapping of pyrolytic carbon and silicon carbide coatings on simulated fuel particles by time-domain thermoreflectance," *J. Nucl. Mater.*, vol. 378, no. 1, pp. 35–39, Aug. 2008, doi: 10.1016/j.jnucmat.2008.04.007.
[20] T. Wang, Z. Gui, A. Janotti, C. Ni, and P. Karandikar, "Strong effect of electron-phonon interaction on the lattice thermal conductivity in 3C-SiC," *Phys. Rev. Mater.*, vol. 1, no. 3, p. 034601, Aug. 2017, doi: 10.1103/PhysRevMaterials.1.034601.
[21] P. Lee, R. Yang, and K. Maute, "An Extended Finite Element Method for the Analysis of Submicron Heat Transfer Phenomena," in *Multiscale Methods in Computational Mechanics*, vol. 55, R. de Borst and E. Ramm, Eds. Dordrecht: Springer Netherlands, 2011, pp. 195–212. doi: 10.1007/978-90-481-9809-2_11.
[22] J. Klett, "Finite-element modeling of heat transfer in carbon/carbon composites," *Compos. Sci. Technol.*, vol. 59, no. 4, pp. 593–607, Mar. 1999, doi: 10.1016/S0266-3538(98)00099-2.
[23] "Stabilization of the no-motion state in the Rayleigh–Bénard problem," *Proc. R. Soc. Lond. Ser. Math. Phys. Sci.*, vol. 447, no. 1931, pp. 587–607, Dec. 1994, doi: 10.1098/rspa.1994.0157.
[24] J. K. Farooqi and M. A. Sheikh, "Finite element modelling of thermal transport in ceramic matrix composites," *Comput. Mater. Sci.*, vol. 37, no. 3, pp. 361–373, Sep. 2006, doi: 10.1016/j.commatsci.2005.11.001.
[25] J.-M. Goyhénèche and A. Cosculluela, "A Multiscale Model for the Effective Thermal Conductivity Tensor of a Stratified Composite Material," *Int. J. Thermophys.*, vol. 26, no. 1, pp. 191–202, Jan. 2005, doi: 10.1007/s10765-005-2366-y.
[26] C. Lorrette, "Outils de caractérisation thermophysique et modèles numériques pour les composites thermostructuraux à haute température," p. 243, 2007.
[27] W. J. Parker, R. J. Jenkins, C. P. Butler, and G. L. Abbott, "Flash Method of Determining Thermal Diffusivity, Heat Capacity, and Thermal Conductivity," *J. Appl. Phys.*, vol. 32, no. 9, pp. 1679–1684, Sep. 1961, doi: 10.1063/1.1728417.
[28] J. Ahrens, B. Geveci, and C. Law, *ParaView: An End-User Tool for Large Data Visualization - Visualization Handbook*. Elsevier, 2005.
[29] B. Qiu, J. Wang, Y. Deng, M. Wang, Y. Wu, and S. Z. Qiu, "A review on thermohydraulic and mechanical-physical properties of SiC, FeCrAl and Ti3SiC2 for ATF cladding," *Nucl. Eng. Technol.*, vol. 52, no. 1, pp. 1–13, Jan. 2020, doi: 10.1016/j.net.2019.07.030.
[30] M. Murabayashi, S. Tanaka, and Y. Takahashi, "Thermal Conductivity and Heat Capacity of Zircaloy-2, −4 and Unalloyed Zirconium," *J. Nucl. Sci. Technol.*, vol. 12, no. 10, pp. 661–662, Oct. 1975, doi: 10.1080/18811248.1975.9733170.
[31] M. A. Snead, Y. Katoh, T. Koyanagi, and G. P. Singh, "SiC/SiC Cladding Materials Properties Handbook," ORNL/TM--2017/385, 1399957, Aug. 2017. doi: 10.2172/1399957.
[32] P. Tao and Y. Wang, "Improved thermal conductivity of silicon carbide fibers-reinforced silicon carbide matrix composites by chemical vapor infiltration method,"

Ceram. Int., vol. 45, no. 2, pp. 2207–2212, Feb. 2019, doi: 10.1016/j.ceramint.2018.10.132.
[33] L. Duquesne, J. Bischoff, V. Chabretou, and C. Delafoy, "Characterization of thermal properties of SiCf/SiC composites for enhanced accident tolerant fuel," p. 7, 2018.
[34] L. Duquesne, C. Lorrette, C. Pradère, G. L. Vignoles, and J.-C. Batsale, "A flash characterisation method for thin cylindrical multilayered composites based on the combined front and rear faces thermograms," *Quant. InfraRed Thermogr. J.*, vol. 13, no. 2, pp. 182–194, Jul. 2016, doi: 10.1080/17686733.2016.1165958.
[35] L. Duquesne, "Caractérisation thermique de structures composites SiCf/SiC tubulaires pour applications nucléaires," p. 173, 2015.